Machine learning pattern recognition algorithms with application to coherent laser combination

Machine learning pattern recognition algorithms with application to coherent laser combination

Dan Wang, Qiang Du, Tong Zhou, Antonio Gilardi, Mariam Kiran, Bashir Mohammed, Derun Li, Russell Wilcox

***Abstract*—Coherent beam combined (CBC) lasers require feedback stabilization of many optical phases, which can be accomplished using machine learning (ML) to recognize phase errors from characteristic interference patterns. Several ML algorithms have been developed as deterministic and fast feedback methods to control CBC lasers. However, learning is difficult when the initially unstabilized phases are constantly drifting. Here, we introduce a novel and general solution to the problem of teaching an ML model to recognize patterns and derive error information from an unstable system, and apply it to spatial and temporal coherent optical combinations. This scheme also provides for learning during operation in order to track changes. Instead of learning absolute values of observation and action in phase space, the ML model learns differential values quickly while the phases drift. Simulations of feedback stabilization demonstrate this new learning method works for both diffractive spatial combining and temporal stacking, and scales to 81-beam spatial combining while maintaining high stability and efficiency.**

***Index Terms*—Machine Learning, Photonic Signal Processing, Pattern Recognition, Neural Network, Phase Drift, Coherent Beam Combination, Control**

I. Introduction

Coherent beam combining (CBC) is a promising technique for laser power scaling, and is key to a broad range of applications [1], [2], [3]. Laser energy can be combined in different ways, including temporal pulse stacking [4] and spatial beam addition using schemes such as binary tree [5], tiled aperture, and filled aperture diffractive combining [6], [7], [8]. In all cases, it is imperative that the coherence of the whole beam array be maintained against environmental perturbations using an active stabilization controller [9], [10], [11]. Often, there are challenges to identify errors and build a deterministic error detector.

Control challenges in complex CBC lasers include large dimensionality in the control parameters. For example in a two-dimensional, N×M beam combination system with a diffractive optical element [8], [12], the number of input phase control variables is N×M, and the output/observable variables include (2N-1)×(2M-1) beams in an interference pattern. Optical coherence stabilization requires fast control to suppress noise from the environment with high bandwidth [12]. Also, measurement of laser intensity loses phase information when using an optical power measurement from cameras or photodiodes, thus phase information must be retrieved with an iterative process and this tends to be slow [13]. Another consequence of measuring optical power is that there might be nonlinear response and non-unique input conditions for each output pattern, making model-based active control difficult.

Stochastic parallel gradient descent (SPGD) is a general and commonly used solution for CBC lasers control, which uses a simple, single detector [10], [7]. SPGD finds phase errors by dithering the input phases and measuring combined beam power to search for the right direction to move in phase space. The number of correction steps SPGD takes to converge is approximately ten times the number of combined beams [11], which slows down when scaling to many beams. Most importantly, SPGD introduces noise in the output power by its need for dithering and searching, adding noise to operational systems [12].

Machine learning control (MLC) is a promising technique to provide the controls needed for complex systems [14]. MLC solves optimization control problems using machine learning (ML) methods. It takes advantage of both the data-driven field of ML and well-developed methods from control theory, and has already led to many exciting ideas and innovative applications in complex nonlinear systems [15], [16], [17]. Some preliminary results have indicated the value of MLC in complex CBC lasers. For the unsupervised approach, a deep reinforcement-learning (RL) controller has shown promising capabilities when applied to 2-beam spatial combination [18], with more beams combined in simulations [19]. A new algorithm combined RL with SPGD to demonstrate robust control in simulations with 128 beams in temporal combination [20]. With an RL controller, 100 beams have been spatially combined in a simplified experimental setup, using two spatial-light-modulators [21]. For supervised MLC, our previous work solved the problem of non-uniqueness of patterns, and showed that a simple, fully-connected neural network (NN) can be trained to combine 81 beams using interference pattern recognition in simulations [22]. However, while there is progress with MLC in CBC lasers, there are also significant challenges.

The lack of labelled data for training prevents pattern recognizing MLC from being applied to real systems [22]. Because most coherent combination systems depend on uncontrolled parameters which slowly drift [23], a machine trained to control the system in one state of key parameters may not be able to control the system if those parameters change. There is also the problem of training the machine initially: if the system is not stable, then the absolute value of the input and output is always unknown due to random perturbations from

This work is supported by the Office of Science, Office of High Energy Physics, of the U.S. Department of Energy under contract no. DE-AC02-05CH11231.

The authors are with the Lawrence Berkeley National Laboratory, 1 Cyclotron Road, Berkeley, CA 94720, USA. e-mails: (dwang2@lbl.gov; qdu@lbl.gov; tongzhou@lbl.gov; antonio.gilardi@lbl.gov; mkiran@es.net; bmohammed@lbl.gov; dli@lbl.gov; rbwilcox@lbl.gov).

the environment, and it will drift away with time. How can we label the inputs and outputs for the ML model to learn?

In this paper, we solve these problems by training the machine using pairs of measurements separated by a known step change of input phase, performed quickly enough so that random drift is small by comparison. We call this the "deterministic differential remapping method (DDRM)". We show that this general approach can be used to control coherent beam combination by recognizing interference patterns and adjusting optical phases, providing robust and low-noise stabilization of the output beam power. DDRM in pattern recognition enables machine learning models to learn on unstable systems as a general approach in different applications.

The approach presented in this paper is a general solution for machine learning controls in CBC lasers, and it has been experimentally demonstrated specifically in a diffractive spatial combining system, with less than one percent stability [24], [25]. This paper explores the details of this approach in simulations, as well as demonstrating generalization to different CBC lasers with different learned patterns.

We first show how phase drift causes failure to label patterns in Sec. II. We then introduce the deterministic differential remapping method (DDRM) in Sec. III, which addresses the problem of making the neural network (NN) approach robust against system drift. Sec. IV presents a general way to implement DDRM in a feedback loop, and also an incremental learning process based on DDRM. Sec. V introduces the sampling method to obtain the NN training dataset. Sec. VI shows the performance of DDRM NN-based feedback, both on a 9-pulse, 4-cavity temporal pulse stacker [4], and an 8-way, 2D diffractive combiner [8], [12], where we analyze the combining efficiency and stability of the scheme. Sec. VII shows an example of how this approach is applied to a large-scale case of 9×9, 81-beam 2D diffractive combing in simulation.

II. Pattern Recognition in CBC and its Challenges from Phase Drift

Coherent beam combiners can serve as mapping functions from laser beam phase space to an interference pattern intensity space. Here we assume we only have photodiodes to measure the pulse intensity in temporal stacking, and only a camera to look at the interference patterns in diffractive spatial combining. Those sensors are easily implemented in optical setups, while providing incomplete measurements that lose the output phase information.

The pattern recognition process used for control is the reverse of the combining process, in that we need to recognize the control variable of input beam phases based on intensity patterns. We have shown that deterministic stabilization can be achieved by pattern recognition after characterizing the transmission function of the combiner optic. A two-dimensional beam array has been experimentally combined with high efficiency, utilizing a physical model of the system, including 8 beams in an 3×3 array [12], and 81 beams in an 9×9 array [26]. Alternatively, it is desirable to implement a controller without having knowledge of the combiner itself. A machine learning controller has proven to be an effective solution where the mapping information can be learned from experimental data. It was shown that a simple, fully connected neural network (NN) can be trained to combine 81 beams [22] from diffractive pattern recognition. We have also shown previously in coherent spatial beam combining that the problems of non-uniqueness of the output state and large numbers of dimensions associated with increased beam number can be mitigated by training only on data from a limited range of phase space [22].

There are other problems with the simplified approach outlined above. One is that we need to train the NN on a drifting system. If the system could be completely trained before any significant drift, that would work, but with the current sample rate (1kHz) this is not possible. Several thousand samples are required and with a sample time of 1ms this requires several seconds, during which time the drift will be unacceptable [23].

Figure 1 shows the large error from accumulated phase drift if we try to label the absolute value of phase during pattern recognition (Fig. 1a). One thousand samples exhibit a large random phase drift value from the original setting, thus the real absolute value of phases is unknown. In contrast, we see a relatively small error from drift when we only label adjacent samples (Fig. 1b), which is the basis of our Deterministic Differential Remapping Method (DDRM) as discussed below. For a realistic case, phase drift is only a few degrees during millisecond sample delay [24].

The other problem is that parameters not controlled by the phase actuator (such as relative beam power) change during long term operation and cause the phase/pattern correlations to change. Similar to phase drift, error from uncontrolled parameters is also small when we only label adjacent patterns during a short sample delay.

III. The Deterministic Differential Remapping Method (DDRM) for Pattern Recognition

Here we present the machine learning approach of Deterministic Differential Remapping Method (DDRM), which addresses above challenge of phase drift in pattern recognition. In DDRM, instead of learning the absolute value of observation and action, we let the ML controller learn differential values in unstable systems. In this case we input a known action, observing the result before and after. During feedback control, we feed the ML a current measurement together with a target pattern (with the highest combining efficiency), and the ML predicts the action needed to move the system between the two states in a deterministic way. In other words, we opted to solve these problems by training the NN to correlate pattern differences with phase differences, so that we can train on a drifting system and then retrain during operation in order to track changes. The NN becomes a device which learns which differences in interference patterns are correlated with which vectors in phase space (control variables' space), so that given an ideal pattern, it can find the error vector for feedback.

Fig. 2a shows the training process. Since the absolute beam phase state is unknown due to drift, we can inject a known

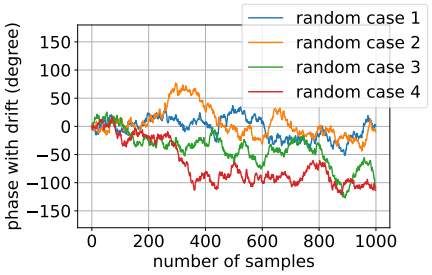

(a) 4 random cases indicate that drift accumulate during sampling time and change the absolute value of phase in a random way.

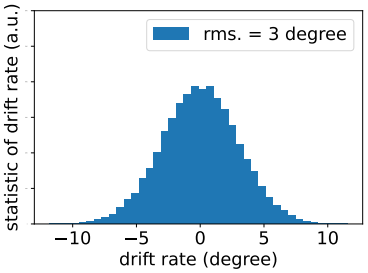

(b) For above 4 cases, the statistic of drift rate, i.e., the drift amount during two adjacent samples

Fig. 1: example show large error from accumulated phase drift (a) and relatively small error from drift rate (b)

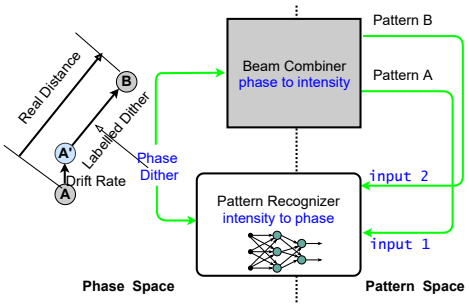

(a) DDRM-based training. (A) and (B) in phase space correspond to pattern A and pattern B in pattern space, which are learned states by the NN. We label the phase distance between (A) and (B) as the injected dither, which has an error from the random dither rate during sampling delay, as the state (A) drifts to state (A')

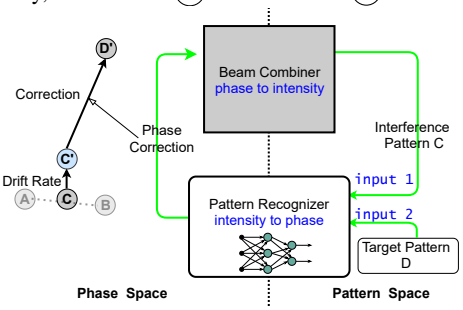

(b) DDRM-based feedback, (C) and (D') in phase space correspond to current pattern C and near-target pattern D' in pattern space. The distance/correction needed between those states can be predicted by the trained NN with errors from prediction error. Correction is also affected by the random drift rate, due to sampling/feedback delay as state (C) drifts to state (C')

Fig. 2: DDRM-based training and feedback. a: training the NN with two patterns and a corresponding phase dither in between. b: feedback by correcting a predicted phase error between the current pattern and target pattern. The measured intensity patterns on the right sides of the figures are associated with the circled phase states shown at left.

phase dither and measure the diffraction patterns before and after (pattern A and pattern B), with the time interval ϵ between 2 frames. Then we can build up a mapping between the phase space and the pattern space using the correlated data samples of [pattern A, phase dither, pattern B]. In the figure, (A) and (B) are states in phase space, which correspond to pattern A and pattern B in pattern space. They are the labelled states for NN training. There is an error in the labelled phase dither between A and B, (A) drifts to state (A') due to the random drift rate within 2 samples. And the drift rate is small as shown in Fig. 1b.

The dither vector is a random sample from an n-dimensional space, with the RMS value of σ_{dither} for a set of selected samples. The vector is drawn from uniformly distributed orthogonal matrices generated by the special orthogonal group $SO(n)$, which is widely used in many numerical applications including Monte-Carlo methods for best sampling efficiency in a high-dimensional data space. The generated vectors will be statistically independent variables having zero mean and equal variances. This is the same as is being used in Stochastic Parallel Gradient Descent (SPGD) algorithms for CBC [11].

The unknown drift function is random and time varying, which changes the absolute value of system phase continuously. Here we are concerned about the drift rate as we measure successive intensity patterns. The RMS value is σ_{drift} for a set of picked samples, which is fixed for a given system and given sampling speed. For most cases, the drift rate is small. For example, in the pulse stacking experiment we control at 1.2 kHz, which corresponds to a feedback delay less than 1 millisecond on a a field-programmable gate array (FPGA). The drift rate is less than 40 mrad per cavity [27].

In our 8-beam diffractive combining experiment, the feedback delay is about 4 milliseconds when we operate the feedback control on a CPU without hardware acceleration, and the natural drift rate is 3.5 degrees [24]. In our simulations, we can tune the value of the drift rate to explore the capability of the algorithms.

Highly accurate prediction by the trained NN can be achieved if the dither speed is much faster than the natural drift rate, by reducing the sampling period ϵ or increasing the dithering amount, so that the drifting contribution can be made negligible during training. Thus we require: $\sigma_{\text{dither}} \gg \sigma_{\text{drift}}$ for the training dataset, i.e., the RMS dither amount σ_{dither} is larger than the RMS value of unknown drift $\sigma_{\text{drfit}}(t)$. But σ_{dither} can't go beyond the range of $([-\pi/2, \pi/2])$ around the optimal state, to avoid pattern ambiguity in the full 2π range [22].

In summary, in the training process, if the dither speed is much faster than the drift rate, there are mappings between phase space and pattern space: [pattern A, pattern B] to [applied dither vector].

Fig. 2b shows the feedback process, where the trained

neural network predicts the distance vector in phase space from any given pair of pattern space samples. For coherent combining stabilization it is important to have the best achievable combining efficiency, which corresponds to a target diffraction pattern D. We find a target pattern (one with highest combining efficiency) in the training dataset and use it as the destination (an input to the neural network) together with a measured current pattern C, which corresponds to an arbitrary phase state Ⓒ. Although Ⓒ may not have been seen in the training dataset, the inference of the neural network acts as a multidimensional interpolation to predict the distance vector to the target state D from its experience of Ⓐ and Ⓑ , given that the sampling grid is smaller than the discontinuity of the multidimensional landscape. Because of the delay of feedback ε, the beam phase state may have drifted away from the phase state Ⓒ to Ⓒ' by the time the feedback is applied, resulting an inaccurate correction. This leads to a near-target pattern D' instead of the exact target pattern D, due to errors from NN predictions as well as random drift rate. These errors result in combining efficiency instability. A larger feedback delay leads to a larger instability and lower combining efficiency. This is a common problem for all feedback control systems, and can be mitigated by introducing a controller such as a simple proportional–integral–derivative (PID) controller [28] or a Kalman filter [29], which is more tolerant to measurement inaccuracy. Here in the simulations we simplified the feedback delay, making it equal to the sampling time interval ϵ, and the PID controller is only proportional without integral and derivative.

In summary, in the feedback process, the NN pattern recognizer acts as a multidimensional phase detector and the correction vector is predicted from a pair consisting of a target pattern and a measured pattern. The combiner phase state is stabilized close to optimal, a state which has the highest combining efficiency seen from the training dataset.

IV. DDRM IN FEEDBACK LOOP AND INCREMENTAL LEARNING

This DDRM method can be applied to any type of coherent combining control, including temporal combining and spatial combining, and can be extended to generic multi-in-multi-out control feedback systems.

Fig. 3 shows how the DDRM algorithm-based neural-network and iteration is implemented in a feedback loop, with one whole cycle around the loop counting as one feedback step. We take the in-time interference pattern together with a target pattern (ideal pattern) as input into the trained NN. The NN recognizes the phase error between the patterns, and sends error signals to the PID controller which applies a phase correction to bring the current pattern toward the target pattern. The laser beams' phase is then updated, and a new interference pattern is generated and so on. Once the phase matrix is close to the optimal point, the phase correction from the NN recognition algorithm is always less than the prediction errors, i.e., always keeping the optimal/stable state within a given tolerance during the iterative process.

We now show that the training samples can be from the recorded observation and action pair of any existing controller that can roughly maintain the optimal combining state. Such a controller can be a popular SPGD process [11], or the neural network based controller itself, which in turn becomes a continuous relearning process that can capture and track the system variations as shown in Fig. 3.

For incremental learning, we keep the original trained NN models and introduce new data from the feedback process. As long as the phase correction signal is larger than the drift rate, the data includes new information and can be used to update the trained model and track changes in uncontrolled parameters.

V. SAMPLING METHOD FOR DDRM TRAINING

As mentioned above, samples used to train the NN models must be within ($[-\pi/2, \pi/2]$) around the optimal state, to avoid pattern ambiguity. Also, the RMS dither σ_{dither} must be much larger than the RMS drift rate σ_{drift} in order to have high signal-to-noise labelled data for NN training. As reported in Ref. [30], randomly chosen samples can be used when drift is slow (drift rate σ_{drift} <6 degree) as we start from the optimal state. This selection criterion fails for fast drift($\sigma_{\text{drift}} \geq 8$ degree), as even for a small number of samples the system drift would bring phase over the π range. Thus we use a selected sampling method which only selects patterns near optimal as samples to train the NN and rejects patterns with low combining efficiency in order to avoid ambiguity. In practice, closeness to an optimal state can be maintained and samples can be selected while using an SPGD controller and the incremental learning process as discussed above [24].

500 samples are used in the diffractive combining simulation, with a system drift rate of 4 degree per sampling interval, and the RMS dither amount σ_{dither} of 30 degree for the initial exploration with selected samples. The RMS error between the predicted phase and the known phase drops as we train the NN as shown in Fig. 4a. We then take training data based on the incremental learning process and plot the training curve as shown in Fig. 4b, where new data is obtained from the corrections against system drift and thus in a very limited phase range. During incremental learning, new data updates the trained NN model, thus producing a clear drop of the RMS error.

The values of the RMS errors in Fig. 4 are not directly relevant to the final combining efficiency and stability because they come from the NN training process, which compares the labelled data with the fitting data. Since our measured/labelled phase neglects system drift while the real one includes system drift, to really evaluate the prediction error of the NN model during feedback we need to test the model with data with a drift range as discussed in the following section.

VI. PERFORMANCE AND STABILITY ANALYSIS

We have simulated 3 types of NN that have been trained in different applications; 3x3 diffractive combining, 9-beam temporal stacking, and 9x9 diffractive combining. In each case the NN differs, as well as different scanned parameters including dither range and drift rate. For a given parameter-set and a given case, the trained NN model can always be reproduced by running the same simulation code.

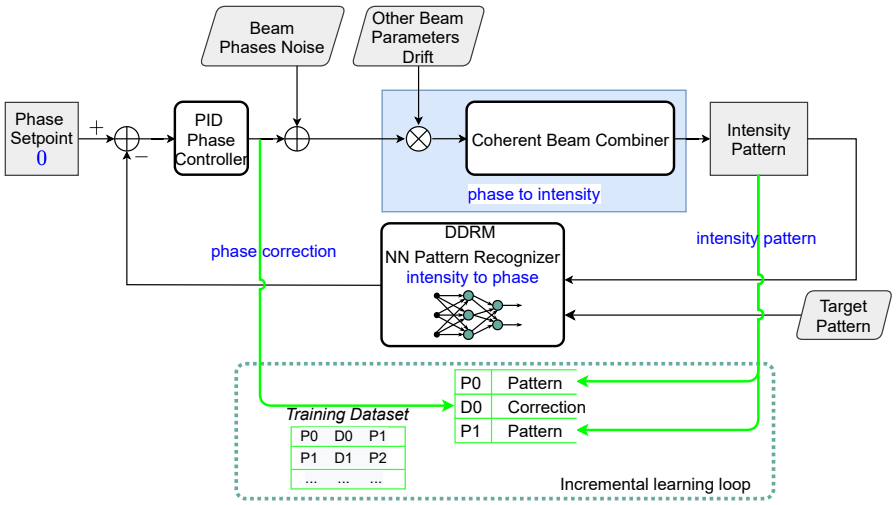

Fig. 3: General way of implementation of the interference pattern recognition machine learning algorithm in CBC lasers, with DDRM-based approach, NN models trained with double-state dither, in a stabilized control loop robust against phase drift. The trained NN takes a static target pattern, together with a measured pattern, and predicts the phase vector in between, which can be used for feedback. The recorded data pair is used for the relearning process.

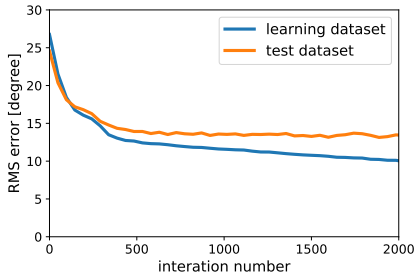

(a) NN model with selected samples, with RMS dither range in 30 degrees and the RMS drift rate 4 degrees.

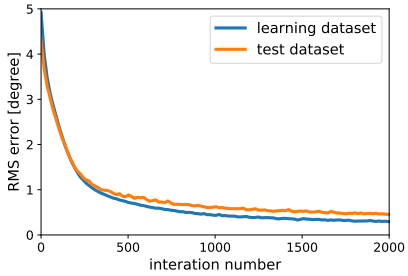

(b) NN model in the incremental learning process, with new samples obtained from NN-based controller as shown in Fig. 3

Fig. 4: RMS error of NN models for learning samples and test samples

Data used for training is always generated from scratch by running the simulation code based on the physics model presented in Sec. VI-A for temporal stacking and in Sec. VI-B for diffractive combining.

The outcomes of the training, testing and validation differ for different NN types, training methods and different parameters used, although the convergence trends are all similar as shown in Fig. 4. The drop of the RMS error curves indicate success of training the NN model. Simulations described below indicate that models with selected samples and incremental learning can be successfully applied in a general feedback loop.

As we focus more on performance when implementing the trained NN in feedback control, we use the prediction error to judge performance instead of the direct training curves since the larger prediction error leads to poor stability in the feedback control, as discussed in Sec. VI-C.

A. *feedback in temporal stacking*

The Gires-Tournois interferometer (GTI) based coherent pulse stacking scheme stacks a series of phase-modulated pulses into one, using a series of concatenated cavities [31]. Each cavity is comprised of one low-reflectivity input–output mirror and other high-reflectivity mirrors to form a cavity with a round-trip delay equal to the pulse interval (or a multiple thereof), as shown in Fig. 5a. Characterizing each pulse by the complex electric field amplitude, we write the i^{th} input pulse as $\mathbf{x}_i$ and the output pulse as $\mathbf{y}_i$. The j^{th} G-T interferometer cavity can be modeled as a linear, time-invariant (LTI) filter, defined by:

$$\mathbf{y}_i - r\alpha e^{j\phi_{\text{cav,j}}} \cdot \mathbf{y}_{i-1} = r\mathbf{x}_i - \alpha e^{j\phi_{\text{cav,j}}} \cdot \mathbf{x}_{i-1}. \qquad (1)$$

where i indicates the pulse numbers ($i = [1, 2, ..., 9]$) and j indicate the cavity number ($j = [1, 2, 3, 4]$). r is the mirror e-field reflectivity, α is the amplitude loss per round-trip and ϕ_{cav} is the optical round-trip phase [27]. The optical round-trip phase determines whether the interference is constructive or destructive. Simulation of cascaded 4 cavities with 9 pulses is a 2 dimensional, fourth order LTI system. The intensity $\mathbf{I} = |s(i,j)|^2$ can be measured with a photodiode after each cavity using leaky mirrors.

For the stacking simulations with 4 identical cascaded GTI cavities, we are using parameters list in Ref. [32], with a

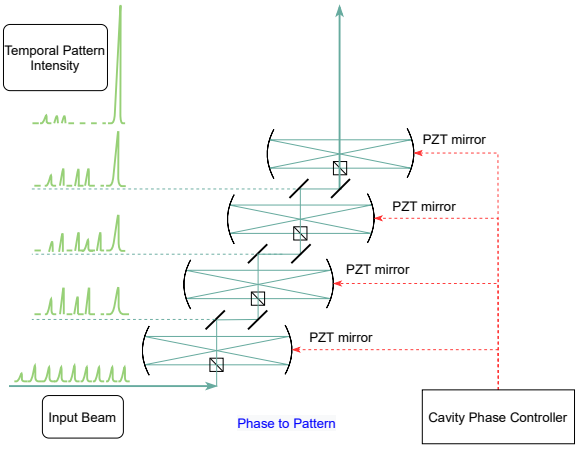

(a) Coherent beam combiner 1: temporal stacking with 9 input pulses and 4 cavities. The combining system corresponds to a mapping function from phase space to interference pattern space.

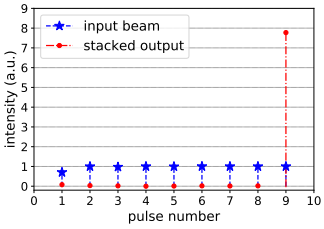

(b) The intensity distribution of input pulses and resulting stacked output. Given a pulse repetition rate, the horizontal axis becomes time.

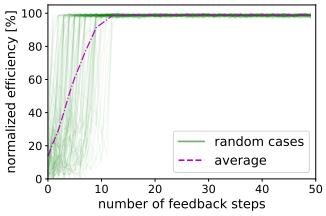

(c) Feedback curves for 100 cases starting from a random state and the average curve, with drift rate 80 mrad per cavity

Fig. 5: DDRM based feedback in temporal stacking

stacking sequence of 9 approximately equal-amplitude pulses. The ideal stacked output intensity versus the input intensity for our setup is shown in Fig. 5b.

The absolute pulse stacking efficiency is defined as: $\eta = \frac{^{\text{out}}I(N)}{\sum_{n=1}^{N} {}^{\text{in}}I(n)}$. For our control study, we didn't optimize the absolute combining efficiency by optimizing the optical parameters (e.g. mirror reflectivities), but just present the feedback efficiency normalized to the maximum achievable from our current models.

Perturbation and random drift is introduced in the simulations which generate samples for NN training. The trained NN recognizes errors and corrects the cavity phase based on temporal intensity patterns. We can either use all the intensity patterns from 4 cavities, or we can just look at the final intensity pattern to determine the phase errors. The former approach needs fewer samples to get the same accuracy since it has more information.

500 samples are used in the NN training, and Fig. 5c shows how the trained NN is applied to correct the intensity pattern to the optimized one, where the maximum peak power enhancement factor is close to 8. The system has a drift rate of 80 mrad in this simulation, which leads to an instability about 5%. And this agrees with the analysis in Ref. [33]. A larger drift rate will cause larger instability in a way similar to the diffractive combining system discussed in the following section.

B. feedback in diffractive combining

We are using an 8-way combiner configuration as in Ref. [12]. The physics process of 2D diffractive combining can be represented as a discrete 2D convolution [12], [5], [8]:

$$s(i,j) = b(i,j) * *d(i,j). \tag{2}$$

where $b(i,j)$ is the input beam function, $d(i,j)$ is the intrinsic DOE transmittance function, and $s(i,j)$ is the corresponding complex far field of the diffracted beam and the intensity $\mathbf{I} = |s(i,j)|^2$, here (i,j) is the horizontal and vertical coordinate of both the input beam array ($i,j = [-3,-2,...0,...2,3]$), and the far field diffracted beam array from the incident direction, with zero-order beam located at (0,0). In general, as 2D convolution suggests, for $N \times N$ inputs and $N \times N$ shaped $d(i,j)$, there will be $(2N-1) \times (2N-1)$ outputs. For the 3×3 input beams as shown in Fig. 6a, the output pattern is a 5×5 array. In the case of of 9×9 diffractive beam combining, the output pattern is a 17×17 array [26].

The simulated 8 input beams have equal amplitude, and the ideal input beam phases match the DOE transfer function such that: $\angle b(i,j) = -\angle d(-i,-j)$, where $\angle$ stands for the phase function [8], [12]. Still, for the control studies we only present the normalized combining efficiency, which is the ratio of the central combined beam power to the maximum achievable central power with the ideal input beam phase case.

We introduce phase perturbation and random phase drift in the simulations, which cause initial low combining efficiency. Then we use the trained NN to recognize errors and correct

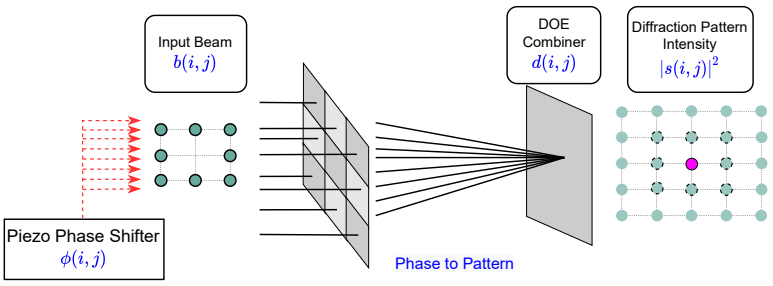

(a) Coherent beam combiner 2: spatial combining with diffractive optical element (DOE) for a 3 by 3 input beam array. The combining system corresponds to a mapping function from phase space to interference pattern space

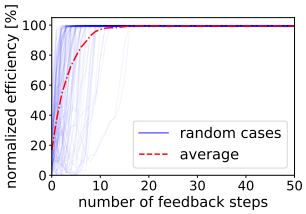

(b) Feedback with drift rate: 4 degrees

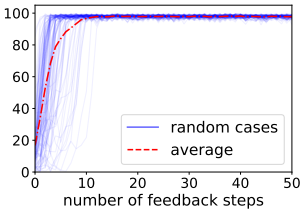

(c) Feedback with drift rate: 8 degrees

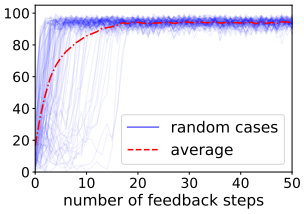

(d) Feedback with drift rate: 12 degrees

Fig. 6: DDRM based feedback in diffractive combining

the phase to bring the current state back to the target pattern, thus the maximum efficiency. Feedback curves are shown in Fig. 6b, Fig. 6c and Fig. 6d, with 100 random cases and an average curve in each plot. 500 samples are used to train the NNs. We apply different NN models trained with different dither amounts and different drift rates. The larger drift rate requires larger dither amount in the exploration in order to provide high signal-to-noise ratio samples for NN training. It also takes more feedback steps to converge and leads to larger instability after locking/converged. We analyze the stability in Sec. VI-C.

C. *Efficiency and stability analysis*

The combining efficiency η, and the standard deviation of η, i.e., stability after feedback, are strongly related to the RMS phase error of each channel, σ_ϕ. In feedback with NN correction, the sources of phase error come from two sources. One is the NN prediction phase error (RMS value σ_{pred}), and the other is the random drift rate (RMS value σ_{drift}), with a net effect as:

$$\sigma_\phi = \sqrt{\sigma_{\text{drift}}^2 + \sigma_{\text{pred}}^2} \tag{3}$$

Here, σ_ϕ, σ_{pred} and σ_{drift} are uncorrelated vectors with the same dimension. We statistically analyze the NN prediction error σ_{pred}, and the total phase error σ_ϕ, at different drift rates σ_{drift}, in the NN-based feedback simulations of the diffractive combiner (Sec. VI-B). The tested NN models' dither amount was fixed at 30 degrees while drift rate was varied.

Results are shown in Fig. 7a. The prediction error σ_{pred} during feedback operation is found by testing the trained NN models with samples within the correction region (RMS value equal to the RMS drift rate). Each point in the curve corresponds to a NN that is trained with a given drift rate. Results are reproducible when re-running the same simulation code. Based on the prediction error σ_{pred} (shown in blue), we can derive σ_ϕ using Eq. 3 for a given known drift rate σ_{drift}, (shown in red).

It has been shown that η is related to the uncorrelated RMS piston phase errors σ_ϕ (in radians) from each channel, which is approximately: $\eta = 1 - \sigma_\phi^2$ [34]. This approach works well with small perturbations, but is less accurate with larger σ_ϕ. In that case we can statistically derive η versus σ_ϕ as well as the stability from Monte-Carlo simulations of the physical model of our 8-way 3×3 diffractive combing system. For the Monte-Carlo simulations, we corrupted the laser phase with Gaussian-distributed noise of σ_ϕ, and then performed 2D convolution as in Eq. 2. We then derived statistics of combining efficiency and stability from 20k samples. Monte-Carlo results for given σ_ϕ are shown as dashed lines in Fig. 7b

We can also statistically analyze the combining efficiency and the standard deviation of η, i.e., stability after feedback, from DDRM-based feedback runs like those shown in Fig 6b, Fig 6c and Fig 6d. The dither amount was fixed at 30 degrees while drift rate was varied, for 1000 cases starting from a random initial state. Results are shown in Fig. 7b as red dots and blue stars. As the drift rate (amount of random drift between sampled frames) increases, the efficiency drops while the instability increases. The two methods agree with each other, suggesting that the simplified Monte-Carlo model can be used to predict feedback control performance.

VII. Outlook for Scaling

To enable high energy and average power fiber lasers, which is the ultimate goal of this research, the approach we have demonstrated in simulations must scale to large numbers of beams. Here, we scale to 81 beams to test the concept. A 9×9 (81-beam) diffractive combination testbed was previously

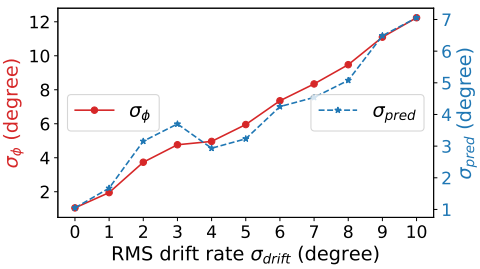

(a) prediction error of NN models σ_{pred}, and the total phase error σ_ϕ, at different drift rate σ_{drift}

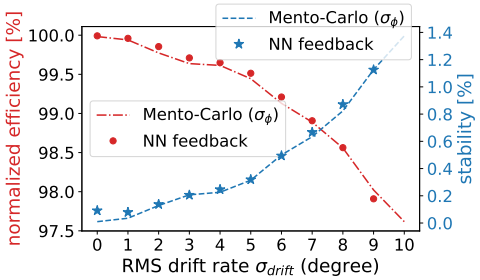

(b) comparison: statistic of NN-based feedback at different σ_{drift} and the Monte-Carlo simulations with σ_ϕ

Fig. 7: Efficiency and stability analysis: sources of total phase error σ_ϕ in DDRM-based feedback (a), and combining efficiency and stability at different drift rates (b).

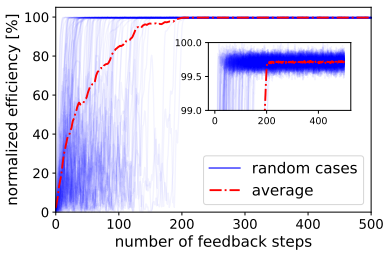

(a) RMS drift rate 5 degree

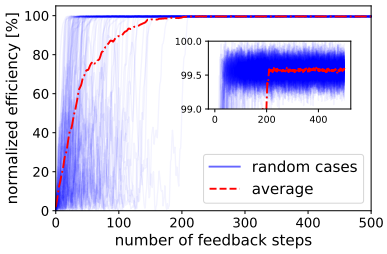

(b) RMS drift rate 10 degree

Fig. 8: Scaling capability of ML based pattern recognition: DDRM-based feedback in 9×9 diffractive combining with different drift rate

developed for tests of control algorithms [22]. We used the same model to test the scalability of the DDRM scheme in simulations.

We train the NN based on the DDRM method with selected samples near optimal. 100k samples are used for NN training and the RMS dither amount is 15 degrees. For NN based feedback, we input the optimal state as the target and correct from any random state. Drift rate is scanned both in the training and test process with 100 random cases, average RMS drift rate 5 degrees and 10 degrees respectively as shown in Fig. 8. The zoomed inset shows the stability and average normalized combining efficiency. For the case of RMS drift rate 5 degrees, the average combining efficiency is 99.7% and RMS stability is 0.08%. For the case of RMS drift rate 10 degree, the average combined efficiency is 99.4% and RMS stability is 1.4%. We see that even at a 10 degree drift rate, the trained NN still works and typically converges in less than 200 steps.

The NN structure for the 9 beam/pulse case (in both diffractive and temporal stacking) is quite simple, with only 3 layers. Both MultiLayer Perceptron (MLP) and Convolutional Neural Networks (CNN) types of neural network can implement DDRM and feedback processes. Structurally, there isn't a significant difference between the two approaches; for 3×3 coherent combining, the input data (double intensity patterns) dimension is $2 \times 5 \times 5$ for CNN, and 1×50 for MLP respectively. For 9×9 combining, we are using a 4 layer MLP with 1×578, (i.e., $2 \times 17 \times 17$) input data.

500 training samples are enough for the 3×3 diffractive beam combining and 9-pulse temporal stacking. For the 81-beam diffractive case, training requires about 100k training samples. The inference latency (i.e. the amount of computation time required to turn a measured pattern into a phase error signal) is similar for both cases. For our 8-beam CBC in a 3×3 array with 5×5 interference pattern, we found the inference time of our 4-layer MLP model is about 0.21 ms, while a CNN model with two convolutional layers is about 0.33 ms on a typical CPU without any GPU acceleration. If the sampling rate (or repetition rate) is increased, e.g. to 10kHz, it is possible to decrease the inference latency by using a hard-real-time edge computer such as an FPGA [35].

Feedback control will correct errors based on previous observations. As system parameters drift away during the latency of feedback, this leads to an intrinsic residual error. Thus a small feedback delay will reduce the residual error. Note that with our control scheme, phase errors are corrected within one sample interval, so that the algorithm itself does not contribute to loop latency. This is not the case with SPGD, where the number of cycles needed to control N beams scales approximately as $10\times$ the number of beams. This is especially important for pulsed lasers operating at kHz rates, because the sample rate is less than or equal to the repetition rate and this determines the control bandwidth. Our scheme can scale efficiently because, as the number of beams increases, so does the amount of information available from the interference pattern. This enables fast error prediction irrespective of the number of beams.

VIII. Conclusion

In summary, we present the deterministic differential remapping method (DDRM) as an innovative solution to address the key challenges of machine learning control in coherent beam and pulse combination, which implements learning on unstable

systems with uncontrolled parameter drift. DDRM recognizes pairs of interference patterns from CBC and implements machine learning-based feedback control. Our scheme is a general solution for feedback control in complex coherent combining systems, recognizing patterns in space or time as shown by feedback in three different types of combiner which are robust against phase drift. This method is scalable regarding the number of beams or pulses, and can support incremental learning during operation. In future work, we intend to experimentally demonstrate that fast computing devices can reduce feedback latency and minimize drift-related errors in the learning process.

REFERENCES

[1] D. J. Richardson, J. Nilsson, and W. A. Clarkson, "High power fiber lasers: current status and future perspectives," *JOSA B*, vol. 27, no. 11, pp. B63–B92, 2010.

[2] M. N. Zervas and C. A. Codemard, "High power fiber lasers: a review," *IEEE Journal of selected topics in Quantum Electronics*, vol. 20, no. 5, pp. 219–241, 2014.

[3] R. Falcone, F. Albert, F. Beg, S. Glenzer, T. Ditmire, T. Spinka, and J. Zuegel, "Workshop report: Brightest light initiative (march 27-29 2019, osa headquarters, washington, dc)," *arXiv:2002.09712*, 2020.

[4] T. Zhou, J. Ruppe, C. Zhu, I.-N. Hu, J. Nees, and A. Galvanauskas, "Coherent pulse stacking amplification using low-finesse gires-tournois interferometers," *Optics express*, vol. 23, no. 6, pp. 7442–7462, 2015.

[5] J. R. Leger, G. J. Swanson, and W. B. Veldkamp, "Coherent laser addition using binary phase gratings," *Applied optics*, vol. 26, no. 20, pp. 4391–4399, 1987.

[6] J. Le Dortz, A. Heilmann, M. Antier, J. Bourderionnet, C. Larat, I. Fsaifes, L. Daniault, S. Bellanger, C. S. Boisson, J.-C. Chanteloup *et al.*, "Highly scalable femtosecond coherent beam combining demonstrated with 19 fibers," *Optics letters*, vol. 42, no. 10, pp. 1887–1890, 2017.

[7] C. Yu, S. Augst, S. Redmond, K. Goldizen, D. Murphy, A. Sanchez, and T. Fan, "Coherent combining of a 4 kw, eight-element fiber amplifier array," *Optics letters*, vol. 36, no. 14, pp. 2686–2688, 2011.

[8] T. Zhou, Q. Du, T. Sano, R. Wilcox, and W. Leemans, "Two-dimensional combination of eight ultrashort pulsed beams using a diffractive optic pair," *Optics letters*, vol. 43, no. 14, pp. 3269–3272, 2018.

[9] T. M. Shay, "Theory of electronically phased coherent beam combination without a reference beam," *Optics Express*, vol. 14, no. 25, pp. 12 188–12 195, 2006.

[10] M. A. Vorontsov and V. Sivokon, "Stochastic parallel-gradient-descent technique for high-resolution wave-front phase-distortion correction," *JOSA A*, vol. 15, no. 10, pp. 2745–2758, 1998.

[11] P. Zhou, Z. Liu, X. Wang, Y. Ma, H. Ma, X. Xu, and S. Guo, "Coherent beam combining of fiber amplifiers using stochastic parallel gradient descent algorithm and its application," *IEEE journal of selected topics in quantum electronics*, vol. 15, no. 2, pp. 248–256, 2009.

[12] Q. Du, T. Zhou, L. R. Doolittle, G. Huang, D. Li, and R. Wilcox, "Deterministic stabilization of eight-way 2d diffractive beam combining using pattern recognition," *Opt. Lett.*, vol. 44, no. 18, pp. 4554–4557, Sep 2019.

[13] J. R. Fienup, "Phase retrieval algorithms: a comparison," *Applied optics*, vol. 21, no. 15, pp. 2758–2769, 1982.

[14] G. Genty, L. Salmela, J. M. Dudley, D. Brunner, A. Kokhanovskiy, S. Kobtsev, and S. K. Turitsyn, "Machine learning and applications in ultrafast photonics," *Nature Photonics*, vol. 15, no. 2, pp. 91–101, 2021.

[15] Y. LeCun, Y. Bengio, and G. Hinton, "Deep learning," *nature*, vol. 521, no. 7553, pp. 436–444, 2015.

[16] Y. Duan, X. Chen, R. Houthooft, J. Schulman, and P. Abbeel, "Benchmarking deep reinforcement learning for continuous control," in *International conference on machine learning*. PMLR, 2016, pp. 1329–1338.

[17] J. Han, A. Jentzen, and E. Weinan, "Solving high-dimensional partial differential equations using deep learning," *Proceedings of the National Academy of Sciences*, vol. 115, no. 34, pp. 8505–8510, 2018.

[18] H. Tünnermann and A. Shirakawa, "Deep reinforcement learning for coherent beam combining applications," *Optics express*, vol. 27, no. 17, pp. 24 223–24 230, 2019.

[19] ——, "Deep reinforcement learning for tiled aperture beam combining in a simulated environment," *Journal of Physics: Photonics*, vol. 3, no. 1, p. 015004, 2021.

[20] A. Abuduweili, J. Wang, B. Yang, A. Wang, and Z. Zhang, "Reinforcement learning based robust control algorithms for coherent pulse stacking," *Optics Express*, vol. 29, no. 16, pp. 26 068–26 081, 2021.

[21] M. Shpakovych, G. Maulion, V. Kermene, A. Boju, P. Armand, A. Desfarges-Berthelemot, and A. Barthélemy, "Experimental phase control of a 100 laser beam array with quasi-reinforcement learning of a neural network in an error reduction loop," *Optics Express*, vol. 29, no. 8, pp. 12 307–12 318, 2021.

[22] D. Wang, Q. Du, T. Zhou, D. Li, and R. Wilcox, "Stabilization of the 81-channel coherent beam combination using machine learning," *Optics Express*, vol. 29, no. 4, pp. 5694–5709, 2021.

[23] S. J. Augst, T. Fan, and A. Sanchez, "Coherent beam combining and phase noise measurements of ytterbium fiber amplifiers," *Optics Letters*, vol. 29, no. 5, pp. 474–476, 2004.

[24] Q. Du, D. Wang, T. Zhou, C. Bakalis, V. Vylta, D. Li, and R. Wilcox, "Stabilizing coherently combined beam power using a robust learning algorithm," in *2021 OSA Laser Congress*, 2021.

[25] Q. Du, D. Wang, T. Zhou, A. Gilardi, M. Kiran, B. Mohammed, D. Li, and R. Wilcox, "Experimental beam combining stabilization using machine learning trained while phases drift," *Optics Express*, vol. 30, no. 8, pp. 12 639–12 653, 2022.

[26] Q. Du, D. Wang, T. Zhou, D. Li, and R. Wilcox, "81-beam coherent combination using a programmable array generator," *Optics Express*, vol. 29, no. 4, pp. 5407–5418, 2021.

[27] Y. Yang, L. Doolittle, A. Galvanauskas, Q. Du, G. Huang, J. Ruppe, T. Zhou, R. Wilcox, and W. Leemans, "Optical phase control of coherent pulse stacking via modulated impulse response," *JOSA B*, vol. 35, no. 9, pp. 2081–2090, 2018.

[28] A. O'dwyer, *Handbook of PI and PID controller tuning rules*. World Scientific, 2009.

[29] G. Bishop, G. Welch *et al.*, "An introduction to the kalman filter," *Proc of SIGGRAPH, Course*, vol. 8, no. 27599-23175, p. 41, 2001.

[30] D. Wang, Q. Du, T. Zhou, C. Bakalis, V. Vylta, D. Li, and R. Wilcox, "Calipr: Coherent addition using learned interference pattern recognition," in *2021 OSA Laser Congress*, 2021.

[31] J. Ruppe, "Theoretical and experimental foundations of coherent pulse stacking amplification," Ph.D. dissertation, 2017.

[32] T. Zhou, J. Ruppe, C. Zhu, I.-N. Hu, J. Nees, R. Wilcox, W. Leemans, and A. Galvanauskas, "Coherent pulse stacking amplification using cascaded and multiplexed gires-tournois interferometers," in *2015 Conference on Lasers and Electro-Optics (CLEO)*. IEEE, 2015, pp. 1–2.

[33] L. A. Siiman, W.-z. Chang, T. Zhou, and A. Galvanauskas, "Coherent femtosecond pulse combining of multiple parallel chirped pulse fiber amplifiers," *Optics express*, vol. 20, no. 16, pp. 18 097–18 116, 2012.

[34] G. D. Goodno, C.-C. Shih, and J. E. Rothenberg, "Perturbative analysis of coherent combining efficiency with mismatched lasers," *Optics express*, vol. 18, no. 24, pp. 25 403–25 414, 2010.

[35] "Xilinx. zynq dpu v3.2 ip product guide," Jul 2020.

Dan Wang received the B.S. degree and the Ph.D. degrees from the Department of Engineering Physics, Tsinghua University, Beijing, China, in 2011 and 2016 respectively. She joined the Accelerator Technology and Applied Physics Division, Lawrence Berkeley National Laboratory, CA, USA, in 2019 and became a research scientist in 2021. Her research interests include machine learning controls, Field Programmable Gate Array, coherent beam combining lasers and accelerator technology.

Qiang Du received the B.S. degree and the Ph.D. degrees from the Department of Engineering Physics, Tsinghua University, Beijing, China, in 2001 and 2006 respectively. He joined the Lawrence Berkeley National Laboratory, CA, USA, in 2013 as a Electronics Staff Scientist / Engineer. His research interests include digital low-level RF control in accelerators, and large scale digital coherence control for multidimensional laser beam combining.

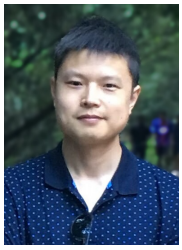

Tong Zhou received the B.S. and M.S. degrees in electrical engineering from Peking University, Beijing, China, in 2007 and 2010, respectively. He received the Ph.D. degree in electrical engineering from the University of Michigan, Ann Arbor, MI, USA, in 2015. He joined Lawrence Berkeley National Laboratory, CA, USA, in 2017 and became a research scientist in 2019. His research interests include energy and power scaling of ultrafast lasers, fiber laser combining, and nonlinear pulse compression.

Antonio Gilardi (Member, IEEE) received a B.S. and M.S degree in Electronics Engineering from the University of Naples Federico II, Naples, Italy, in 2017. He received the Ph.D. degree in electronics with the Department of Electrical Engineering and Information Technology at the University of Naples Federico II, collaborating with the European Organization for Nuclear Research, Geneva, Switzerland in 2021. Currently, he is a post-doc at Lawrence Berkeley National Laboratory, California, USA. His research interests include fiber laser combining, active control system, and particle accelerator technology.

Mariam Kiran received the MSc(Eng) and Ph.D. in Computer Science from University of Sheffield, Sheffield, UK in 2007 and 2011 respectively. She is currently a research scientist and leads the AI for networking group in the Scientific Networking Division at Lawrence Berkeley National Laboratory, Berkeley, California. Her research focuses on machine/deep learning to optimize distributed computing and high-performance networking for complex science workflows in domains of Cloud, optical, 5G and quantum networks.

Bashir Mohammed received the M.S. degree in Control Systems Engineering from the University of Sheffield UK in 2012. He received the Ph.D. in Computer Science from the University of Bradford UK in 2019. He is currently a postdoctoral research scholar in the Computational research division at Lawrence Berkeley National Laboratory. His work focuses on developing ML algorithms to optimally control distributed network resources, improve high-speed big data transfers and avoid network traffic congestion for critical scientific workflows.

Russell Wilcox received the B.S. degree from University of California, Berkeley in 1980. He is a staff scientist in the Accelerator Technology and Applied Physics Division, Lawrence Berkeley National Laboratory, CA, USA, since 2003. His research interests include multi-dimensional coherent beam combined lasers and ultrafast fiber lasers.

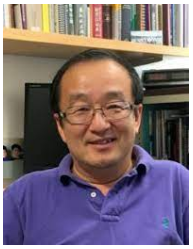

Derun Li received the B.S. and M.S. degrees in Accelerator Physics, Tsinghua University, Beijing, China in 1983 and 1986 respectively. He received Ph.D. degree in physics from Indiana University, Bloomington, IN in 1995. He joined Lawrence Berkeley National Laboratory, CA, USA as a staff scientist in 1997 and is currently a senior scientist and Director of Berkeley Accelerator Controls and Instrumentation Center. His research interests include Accelerator Physics, RF design and modeling, accelerator technologies and controls.